Scramjet Propulsive Flowpath Prediction Improvements Using Recent Modeling Upgrades

Article · January 2005

DOI: 10.2514/6.2005-432

4 authors, including:

James D. Ott
Combustion Research and Flow Technology, Inc.
12 PUBLICATIONS **166** CITATIONS
SEE PROFILE

Kevin Brinckman
Combustion Research and Flow Technology, Inc.
24 PUBLICATIONS **295** CITATIONS
SEE PROFILE

Sanford Dash
Combustion Research and Flow Technology, Inc.
178 PUBLICATIONS **2,030** CITATIONS
SEE PROFILE

Scramjet Propulsive Flowpath Prediction Improvements Using Recent Modeling Upgrades

James D. Ott[†], C. Kannepalli[†], K. Brinckman[†], and S.M. Dash[±]
Combustion Research and Flow Technology, Inc. (CRAFT Tech)
6210 Keller's Church Road, Pipersville, PA 18947
ottjd@craft-tech.com
Phone: 215-766-1520 / Fax: 215-766-1524

Reynolds Averaged Navier Stokes simulations have been performed to examine modeling upgrades for scramjet flowpath predictions. A flush, non-reacting hydrogen fuel injector flowfield was used as the model problem, and an LES simulation of the problem was used for comparison purposes. Calculations were first performed examining the effect of Schmidt number with a constant Prandtl number. Next the effect of the compressibility correction used was examined. These findings indicated that for this injector configuration, the effect of the compressibility had a major impact on the solution, and that the average Schmidt number of about 0.45 compared closely to the LES simulation results. Next, a new scalar fluctuation model was used to obtain local values of Prandtl and Schmidt number whose values were found to vary significantly across the fuel jet mixing layer. The turbulent Prandtl number was found to vary between 0.4 to 0.9, and the turbulent Schmidt number varied from 0.6 to 1.2. Finally, a comparison was performed using an unstructured flow solver with grid adaptation. This technique is now being used to obtain grid resolved solutions in a systematic and straightforward manner in our design studies.

Nomenclature

E	=	Oxygen Entrainment Parameter
K	=	Turbulent Kinetic Energy (m^2/s^2)
K_T	=	Temperature Fluctuation
K_Y	=	Species Fluctuation
T	=	Temperature (K)
u, v, w	=	Velocity (m/s)
x	=	Streamwise Coordinate Direction
Y_i	=	Mass Fraction of species i
δ	=	Boundary Layer thickness (0.1524 cm) / Grid unit
ε, ε_T, ε_Y	=	Turbulent Dissipation
Pr_t	=	Turbulent Prandtl Number, ratio of viscous to thermal diffusion
Sc_t	=	Turbulent Schmidt Number, ratio of viscous to mass diffusion
Le	=	Turbulent Lewis Number, ratio of mass to thermal diffusion
LES	=	Large Eddy Simulation
RANS	=	Reynolds Averaged Navier Stokes

43rd Aerospace Sciences Meeting and Exhibit, Jan. 10-13, 2005, Reno, NV.

[†]Research Scientist, AIAA Member.
[±]President and Chief Scientist, Associate Fellow AIAA

Report Documentation Page

Form Approved
OMB No. 0704-0188

1. REPORT DATE	2. REPORT TYPE	3. DATES COVERED
2005		**00-00-2005 to 00-00-2005**

4. TITLE AND SUBTITLE	5a. CONTRACT NUMBER
Scramjet Propulsive Flowpath Prediction Improvements Using Recent Modeling Upgrades	5b. GRANT NUMBER
	5c. PROGRAM ELEMENT NUMBER
6. AUTHOR(S)	5d. PROJECT NUMBER
	5e. TASK NUMBER
	5f. WORK UNIT NUMBER
7. PERFORMING ORGANIZATION NAME(S) AND ADDRESS(ES) **Combustion Research and Flow Technology Inc (CRAFT Tech),6210 Keller's Church Road,Pipersville,PA,18947**	8. PERFORMING ORGANIZATION REPORT NUMBER
9. SPONSORING/MONITORING AGENCY NAME(S) AND ADDRESS(ES)	10. SPONSOR/MONITOR'S ACRONYM(S)
	11. SPONSOR/MONITOR'S REPORT NUMBER(S)

12. DISTRIBUTION/AVAILABILITY STATEMENT
Approved for public release; distribution unlimited

13. SUPPLEMENTARY NOTES
The original document contains color images.

14. ABSTRACT

15. SUBJECT TERMS

16. SECURITY CLASSIFICATION OF:			17. LIMITATION OF ABSTRACT	18. NUMBER OF PAGES	19a. NAME OF RESPONSIBLE PERSON
a. REPORT	b. ABSTRACT	c. THIS PAGE			
unclassified	**unclassified**	**unclassified**		**14**	

I. Introduction

This paper primarily addresses applying scalar fluctuation modeling to a non-reacting hydrogen fuel injection problem emulating the environment of a hypersonic scramjet combustor. A companion paper [1] discusses details of the modeling and its validation for some unit problems. We briefly review the equations implemented in Section II. In Section III, we describe a detailed LES simulation of this fuel injection problem that builds upon earlier work by Kannepalli et al. [2] and uses recycling/rescaling methodology to interface the LES jet simulation with that of the approach RANS boundary layer. The LES simulation is computationally intensive and has progressed to a state where RMS mean flow quantities are converged but turbulent stresses and scalar variances are still somewhat noisy, but are yielding reasonable values. Extracting local values of Pr_t, Sc_t and Le from the LES simulation entails invoking a gradient transport hypotheses, i.e., σ_α (σ = Pr_t or Sc_t where α is the temperature or species mass fraction respectively) is obtained from

$$\sigma_\alpha = \frac{\overline{u_i'\alpha_i'}}{\overline{u_i'u_j'}} \frac{\partial \overline{u}_i / \partial x_i}{\partial \overline{\alpha} / \partial x_i} \tag{1}$$

where division of second-order correlations is entailed. Thus, σ_α can be very noisy and the LES calculation must be run further to obtain "smooth" values. This is now in progress.

RANS simulations were performed on this same fuel injection geometry with a similar boundary layer inflow profile. Calculations were performed first looking at the effect of Lewis number, using constant values of Pr_t and Sc_t, and then, using the scalar fluctuation equations to provide local values. Calculations were performed with and without a compressibility-correction [3] activated comparing the RANS calculations with the averaged LES data. These comparisons are discussed in Section IV. Our findings are as yet inconclusive, but suggest that modifications to the basic compressibility correction are needed for this class of flows.

Finally, in Section V, we show applicability of our unstructured code, CRUNCH®, to this problem. For realistic applications, CRUNCH® has been used in the fuel injection zones of various scramjet concepts, since the geometry of multiple fuel injection ports is more readily modeled using an unstructured approach. Using the unstructured solver also allows the advantage of our grid adaptation capabilities, which have been found to have a first order effect on parameters such as combustion efficiency, and thus thrust [3].

II. Problem Definition and Computational Methodology

In this section a description of the numerical problem will be discussed. The first part will describe the fuel injection geometry that was used to obtain the numerical results. The part section will describe the initial and boundary conditions for the domain. The last part will describe the methodology of the computational models that were used.

A. Geometry

Figure 1 shows the fuel injection region and channel grid structure. The grid is scaled based on δ, the thickness of the incoming turbulent boundary layer. The channel is 35δ long, 10δ high, and 5δ wide. A flush wall injector, angled at 25 degrees relative to the channel wall, is placed 5δ downstream of the inflow plane along the channel centerline. The injector is a square of 0.5δ on each side. The symmetry plane down the centerline of the injector was utilized so that only half of the domain needed to be modeled. The grid was constructed as one block of 2.8 million cells, with I-blanking. The grid was clustered near the wall and where the injector flowed into the channel.

This same general geometry and gridding was used for both the RANS and LES calculations. The LES calculation does not use the symmetry plane down the middle of the channel, and needed to model the entire channel width of 10δ. Also, due to the expense of the LES calculation compared to the RANS, only 15δ downstream of the injector were modeled. The LES calculation also included a 15δ long and 2δ wide extension upstream on the channel that was used to generate the unsteady turbulent boundary layer.

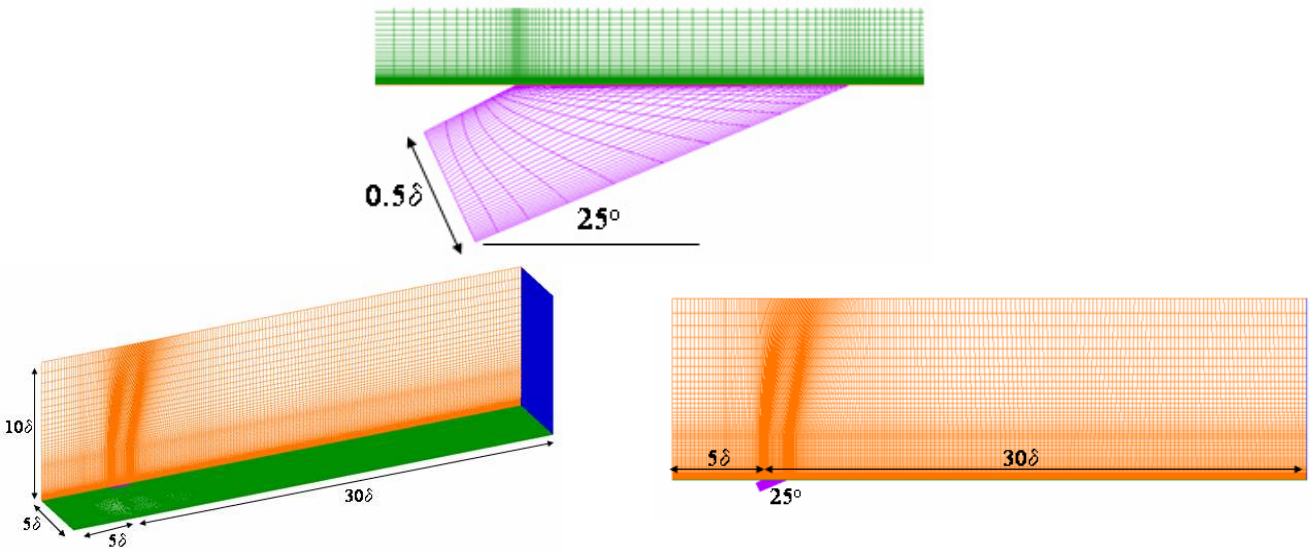

Figure 1. Numerical Model Geometry

B. Inflow and Boundary Conditions

The inflow and injector conditions are given in Table 1. The channel inflow was initialized as air composed of O_2 and N_2, with the species mass fractions of 0.2323 and 0.7677 respectively. A turbulent boundary layer of thickness one δ was created using a $1/7^{th}$ power law distribution for the velocity, and a temperature profile using the Crocco-Busemann relationship [5]. The incoming Mach number, temperature, and pressure are representative of the conditions for the inflow to a scramjet combustor. The injector conditions were set for a pure hydrogen (H_2) inflow at near sonic conditions. The channel wall was a no-slip, isothermal surface having a prescribed temperature of 700K. The y^+ values ranged from 0.2 to 0.4 along the wall surface. The channel exit was a standard extrapolated supersonic outflow.

Table 1. Inflow and Injector Conditions

	Inflow	Injector
u (m/s)	3131.7	1920.0
Mach	4.5	1.05
T_s (K)	1200.0	575.0
p_s (psi)	14.7	325.0
Y_{O2}	0.2323	0
Y_{N2}	0.7677	0
Y_{H2}	0	1

C. Computational Methodology

For this study two CFD codes were used, one using a structured methodology, and the other using an unstructured methodology. The structured code was the CRAFT CFD® solver [4], with Table 2 listing the codes features. This code was used for both the RANS and LES calculations. For the RANS simulations a k-ε turbulence model, shown in Equation 2 and 3, was used with the So-Zhang-Speziale [6] near wall model. A compressibility correction was also available based on a modification to the Sarkar model [7]. The flow was modeled as a non-reacting mixture of thermally perfect gases (O_2, N_2, and H_2).

Table 2. Relevant Features of CRAFT CFD® Navier-Stokes Code

NUMERICS/ PARALLEL PROCESSING	• 1D/2D/AXI/3D Finite-Volume Discretization
	• Implicit, ADI and L/U, Upwind (Roe/TVD) Formulations
	• Fully Implicit Source Terms/Boundary Conditions
	• PNS Run Option
	• Domain-Decomposition Parallel Architecture with MPI
	• Preconditioning Extensions
GRID FEATURES	• Grid Patching/Blanking for Complex Geometries
	• Noncontiguous Grid Interfacing with Flux Preservation Across Domains
THERMO-CHEMISTRY	• Real Gas Mixtures (Calorically and Thermally Imperfect/JANNAF Thermo Tables)
	• Generalized Finite-Rate Chemistry and One-step Option
	• Fully Implicit Source Term Linearization
	• Probability Density Function Turbulent Chemistry Modeling
	• Stiff Chemistry Solver
TURBULENCE	• k-ε / EASM Nearwall Functionality
	• Unified Compressibility and Vortex Stretching Corrections
	• Simplified and Advanced Transition Modeling
	• Particle Dispersion Formulations
	• Hybrid RANS/LES
MULTIPHASE FLOW	• Nonequilibrium Particle/Droplet Solvers (Eulerian and Lagrangian Formulations)
HIGH ALTITUDE MODELING	• Vibrational Non-equilibrium Modeling
	• Slip Wall Boundary Conditions

$$\frac{\partial \overline{\rho} k}{\partial t} + \frac{\partial \overline{\rho} u_j k}{\partial x_j} = \frac{\partial}{\partial x_j}\left[\left(\mu + \frac{\mu_t}{\sigma_k}\right)\frac{\partial k}{\partial x_j}\right] + P_k - D_k + SS_k \tag{2}$$

$$\frac{\partial \overline{\rho} \varepsilon}{\partial t} + \frac{\partial \overline{\rho} u_j \varepsilon}{\partial x_j} = \frac{\partial}{\partial x_j}\left[\left(\mu + \frac{\mu_t}{\sigma_\varepsilon}\right)\frac{\partial \varepsilon}{\partial x_j}\right] + P_\varepsilon - D_\varepsilon + SS_\varepsilon \tag{3}$$

To improve the capability for predicting scalar transport parameters in complex geometries, an earlier temperature variance predictive methodology [8] which operated within the framework of a RANS-based k-ε turbulence model, was extended by Brinkman [1]. The extended model solves for both the temperature and species variance, from which the scalar transport parameters Pr_t and Sc_t are derived. Transport equations for the temperature variance k_T and its dissipation rate ε_T were solved, coupled to the k-ε turbulence model. The transport equations for k_T and ε_T are:

$$\frac{\partial (\overline{\rho} k_T)}{\partial t} + \frac{\partial (\overline{\rho} u_j k_T)}{\partial x_j} = \frac{\partial}{\partial x_j}\left[\overline{\rho}\left(\alpha + \frac{\alpha_t}{\sigma_{k,T}}\right)\frac{\partial k_T}{\partial x_j}\right] + P_{k_T} - D_{k_T} \tag{4}$$

$$\frac{\partial (\overline{\rho} \varepsilon_T)}{\partial t} + \frac{\partial (\overline{\rho} u_j \varepsilon_T)}{\partial x_j} = \frac{\partial}{\partial x_j}\left[\overline{\rho}\left(\alpha + \frac{\alpha_t}{\sigma_{\varepsilon,T}}\right)\frac{\partial \varepsilon_T}{\partial x_j}\right] + P_{\varepsilon_T} - D_{\varepsilon_T} + C_k + \xi_{\varepsilon T} \tag{5}$$

where the compressibility correction accounted for in the k-ε model is carried over with the expression C_k and $\xi_{\varepsilon T}$ is a near-wall damping function included to capture low-Reynolds number behavior. The turbulent Prandtl number with near-wall damping is calculated as

$$Pr_t = \frac{C_\mu f_\mu}{C_\lambda f_\lambda} \sqrt{\frac{k}{\varepsilon} \frac{\varepsilon_T}{k_T}} \tag{6}$$

where f_μ and f_λ are the near-wall damping term for turbulent momentum diffusivity and temperature diffusivity respectively, and C_λ and C_μ are proportionality constants. A similar formulation is implemented for the species mass-fraction variance k_Y and its dissipation rate ε_Y, to calculate a turbulent Schmidt number, Sc_t, and mass diffusivity. For a detailed explanation and definitions of all the variables in equations 5 and 6, see Reference [1].

For LES applications, the CRAFT CFD® [1] solver was implemented with an upwind-biased, Roe-flux-extrapolation procedure that has been extended to fifth order [9,10] for the inviscid and fourth order central differencing for the viscous terms. Temporally, the code includes both a fourth order Runga-Kutta scheme and a second-order three-factor Approximate Factorization (AF) implicit scheme. For the studies described, the AF scheme was used and applied with sub-iterations to remove the splitting error. For subgrid modeling, the code includes a compressible version of the algebraic Smagorinsky model [11] as well as a one-equation model of Menon [12]. The one equation model solves a transport equation for subgrid turbulent kinetic energy, k^{sgs}. The subgrid-scale stresses are then modeled using an eddy viscosity approach based on k^{sgs}. In order to stabilize the code in the vicinity of strong gradients, such as shock waves, a modification of the classic Jameson, et al.[13] 2-4 dissipation scheme was used with a cutoff switch that is tuned to add dissipation only at shocks and discontinuities[2].

For the unstructured simulations, the CRUNCH CFD® [4] solver was used. Table 3 lists these code features. CRUNCH CFD® is a hybrid unstructured RANS solver employing a k-ε turbulence model similar to the CRAFT CFD® solver. The compressibility correction is based on an unmodified Sarkar model[7].

Table 3. Current Features of the CRUNCH CFD® Code

NUMERICS	• Finite-Volume Roe/TVD Flux Construction, Vertex Storage
INTEGRATION	• Explicit Four-Step Runge-Kutta, Implicit GMRES, Gauss-Seidel
GRID ELEMENTS	• Tetrahedral, Hexahedral, Prismatic, Pyramid
PARALLEL PROCESSING CAPABILITIES	• Domain Decomposition MPI, Independent Grids with Noncontiguous Interfacing, Automated Load Balancing
DYNAMIC GRID CAPABILITIES	• Node Movement Solver (Implicit Elasticity Approach), Automated Embedding, Sliding Interfaces
GRID ADAPTION	• Variable Element Grid Refinement using Delaunay and cell subdivision Procedures, Automated Load Balancing of Adapted Grid
THERMOCHEMISTRY	• Multi-component Real Gas Mixtures, Finite-Rate Kinetics
TURBULENCE RANS/LES	• $\tilde{k}\varepsilon$ /EASM Formulations with Compressibility/Vortical Upgrades • LES Subgrid Scale Models – Algebraic and One-equation • Unified Hybrid LES/RANS Framework
MULTIPHASE FLOW	• Nonequilibrium Particle/Droplet Solvers (Eulerian and Lagrangian Formulations), Cavitation Model with Bubble Dynamics

III. LES Simulation

The LES version of the CRAFT CFD® solver was used to solve the 3D fuel jet injection problem. To obtain a turbulent and unsteady boundary layer inflow for the calculation, a computational domain upstream of the main channel was used. A domain length of 15δ in the streamwise direction was required to set up the unsteady supersonic boundary layer via the recycling/rescaling technique [2]. A wall-normal dimension of 10δ and spanwise dimension of 2δ (with periodic boundary conditions) was sufficient to generate a "bona-fide" turbulent boundary layer.

Figure 2 shows a side view along the length of the channel, taken down the centerline of the jet. This figure shows the representative distances at which axial cuts of the domain are taken for comparison purposes. The x coordinate locations shown in the figure are relative to the start of the jet and are in grid units, where 1 grid unit, δ, is representative of the thickness of the incoming boundary layer. The coordinate system origin, x = 0, begins where the injector initially makes contact with the channel wall. Since the injector is at a 25 degree angle with respect to the channel wall, the end of the injector is at about x = 1.5. The channel locations selected for presentation are located at 1δ, 3δ, 5δ, and 7δ. Since the injector was designed to have a diameter of ½ δ, these distances also represent 2, 6, 10, and 14 jet diameters downstream.

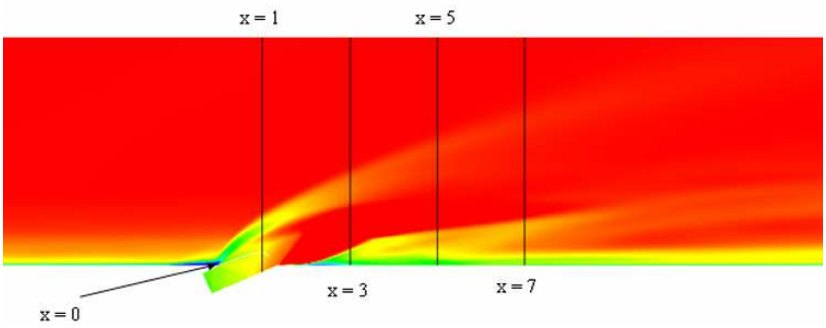

Figure 2. LES Contour Profile Locations.

Figure 3 shows the contours for the mean values of velocity, u/u_∞, temperature, T/T_∞, hydrogen mass fraction, Y_{H2}, turbulent kinetic energy, $\sqrt{K}/ u_\infty$, temperature fluctuation, $\sqrt{K_T}/ T_\infty$, and species fluctuation, $\sqrt{K_Y}$, at the cutting planes defined in figure 2. The turbulent kinetic energy, temperature and species fluctuations are calculated from the LES simulation as:

$$K = \tfrac{1}{2}(\overline{u'u'} + \overline{v'v'} + \overline{w'w'}) \tag{7}$$

$$K_T = \overline{T'T'} \tag{8}$$

$$K_Y = \overline{Y'_{H_2} Y'_{H_2}} \tag{9}$$

Since the LES calculation modeled the entire domain, asymmetry is seen around the jet centerline. These figures show the characteristic vortex formed by a jet entering a supersonic flow. This vortex assists in the mixing of the fuel jet with the airflow through the channel. An additional component of the mixing is due to the mass diffusion of the fuel into the air. Figure 4 shows a three-dimensional view of the LES simulation. The iso-surfaces of temperature (1500 K) are in green, density (0.5 kg/m3) is in orange and the mass fraction of hydrogen (0.5) is in white. The density iso-surfaces show the spherical shock wave structure propagating downstream of the jet. This shock wave fully encloses the injector jet. This figure shows the asymmetry associated with LES simulations.

IV. RANS Simulation with the CRAFT CFD® Solver

The results presented in this section are for the structured RANS solver. Two subsections will be discussed. The first set of calculations look at examining the effect of varying the Schmidt number while maintaining a constant Prandtl number. Also looked at in this subsection is the effect of the compressibility correction on the solution. The second subsection will examine the use of the variable Prandtl and Schmidt number model discussed above, with and without the compressibility correction. Both of these sets of calculations will be compared back to the LES simulation, which will be used like a baseline calculation.

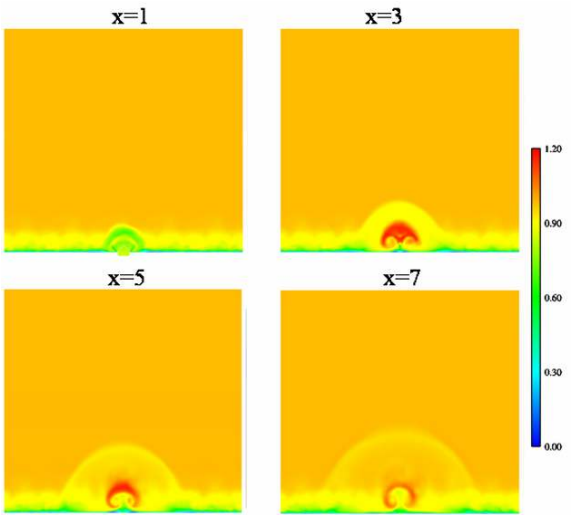

(a). u/u_∞

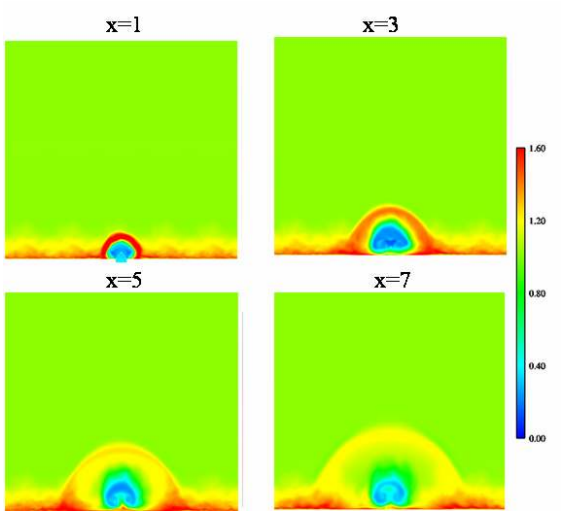

(b). T/T_∞

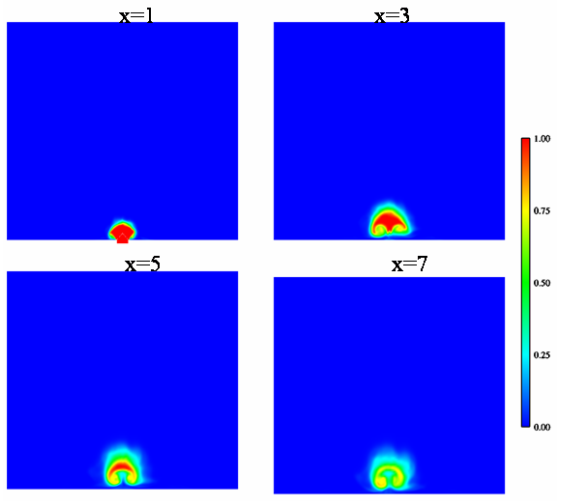

(c). Y_{H_2}

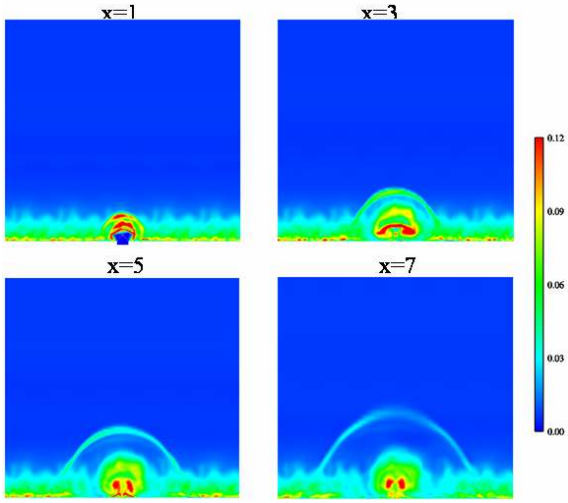

(d). $\sqrt{K}/u_\infty$

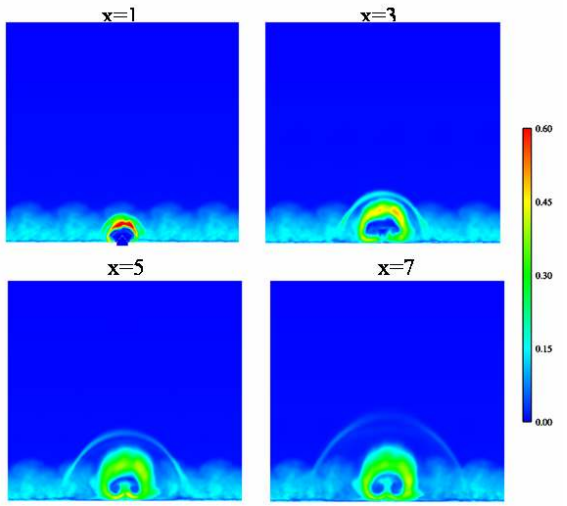

(e). $\sqrt{K_T}/T_\infty$

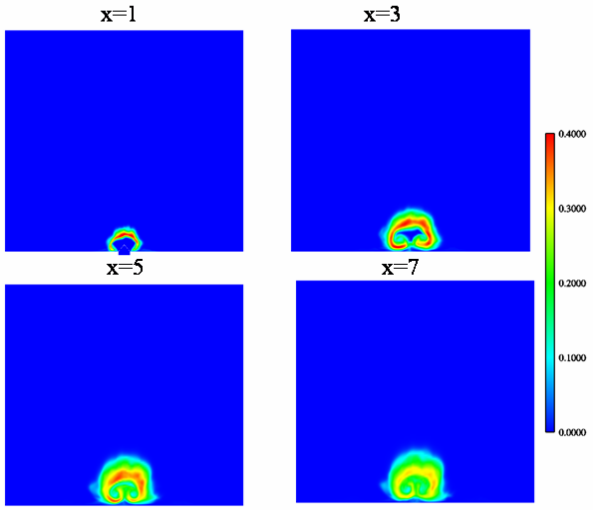

(f). $\sqrt{K_Y}$

Figure 3. LES Profile Contours.

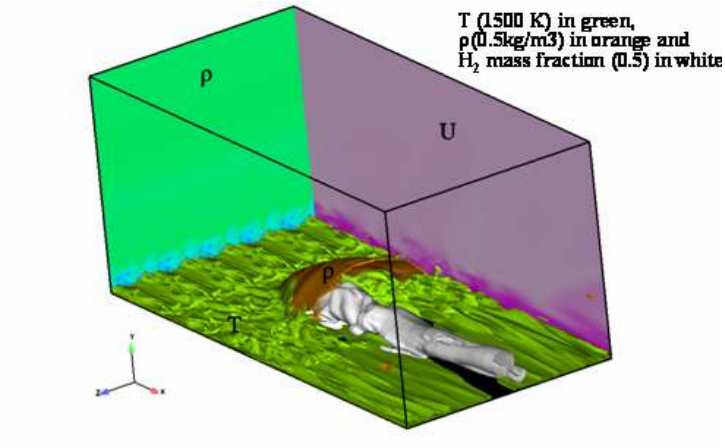

Figure 4. LES Iso-Surfaces.

A. Constant Prandtl Number Calculations

The calculations listed in Table 4 performed with specified values of transport parameters for this study as Cases 1 – 4. The turbulent Prandtl was chosen for all cases to be 0.9, a value that is commonly used for boundary layer applications. The Schmidt number varied between 0.9 and 0.45, making the Lewis number 1.0 or 2.0 respectively. Lowering the turbulent Schmidt number (raising the Lewis number since $Le = Pr_t/Sc_t$) permits the species to diffuse faster than the temperature, which for burning cases can result in earlier burning, see for example Baurle and Eklund[14]. The Schmidt number (or Lewis number) is the parameter controlling turbulent diffusion of the fuel jet into the air stream. The compressibility correction was also a factor considered in this study. This correction suppresses the turbulent mixing rate and reduces the entrainment of air into the jet/air mixing layer.

Table 4. Inflow and Injector Conditions

Case	Compressibility	Pr_t	Sc_t	Le
1	ON	0.90	0.90	1.0
2	ON	0.90	0.45	2.0
3	OFF	0.90	0.90	1.0
4	OFF	0.90	0.45	2.0
5	ON	Variable	Variable	Variable
6	OFF	Variable	Variable	Variable

Figure 5 shows a comparison of the oxygen entrainment shown in into the fuel jet mixing layer for these four constant Prandtl number cases as compared to the value from the LES simulation. The entrainment parameter, E, is defined in Eqn. 10 as the mass flux average of the amount of O_2 that is mixed into the fuel jet. The fuel jet is defined as the computational domain where the mass fraction of fuel is greater than 0.5%.

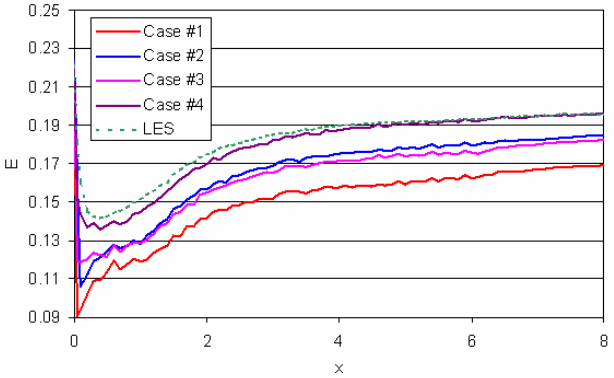

Figure 5. Entrainment of O_2 Into the Jet.

$$E = \frac{\int \rho u_j Y_{O2} dA}{\int \rho u_j dA} \tag{10}$$

Comparing Cases 1 and 2, which have compressibility on, with the Lewis number varying from 1 to 2, the entrainment into the jet is shown to increase due to the increase in mass diffusion, which is keyed to the value of the eddy viscosity divided by the Schmidt number. Comparing Cases 1 to 3, which have the same Lewis number, but the compressibility correction is not used for Case 3, the entrainment increases because the overall mixing is faster since the eddy viscosity itself is larger. Examining the entrainment between Cases 2 and 3 indicates that both faster mixing and increased species diffusivity increase the entrainment by the same magnitude, since the values of the turbulent diffusivity is the same. However, in reacting cases, the effects on the burning may not be the same. Based on the entrainment parameter, the Case 4, which has a Schmidt number of 0.45 and the compressibility correction off, is seen to provide mixing that is comparable to the LES simulation. For this injector configuration, the LES simulation is indicating that compressibility has a major effect, and that the lower Schmidt number produces results more in accord with the LES simulation.

Figure 6 shows a comparison of the four cases at the x=5 cutting plane for the velocity, temperature, mass fraction of fuel, and turbulent kinetic energy. This figure should be compared to Figure 3 a-d for the LES simulation.

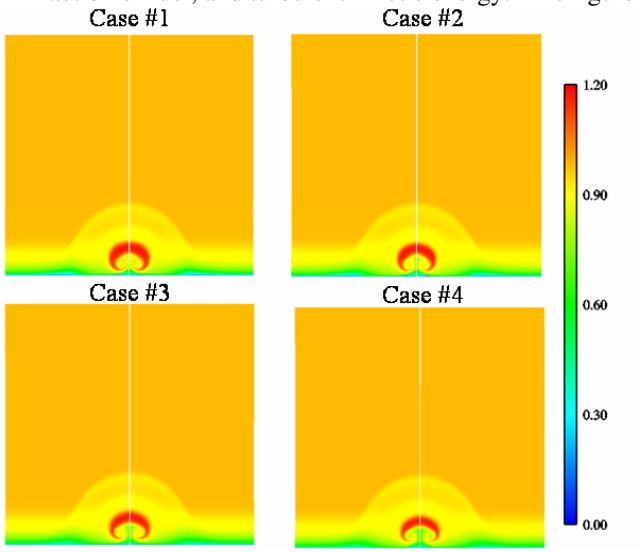

(a). u/u_∞

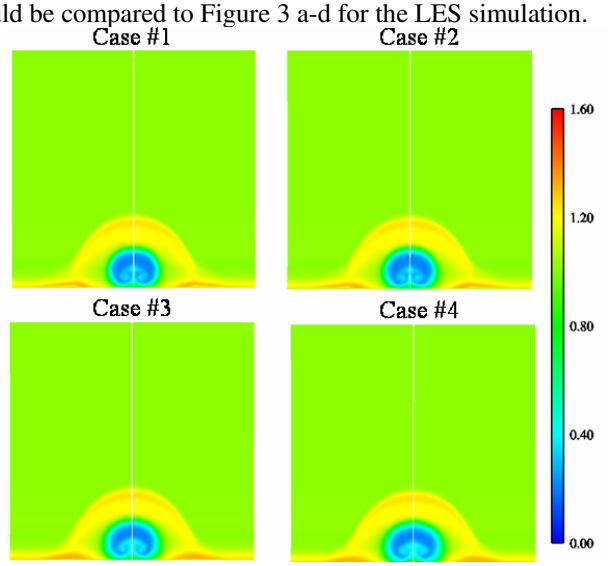

(b). T/T_∞

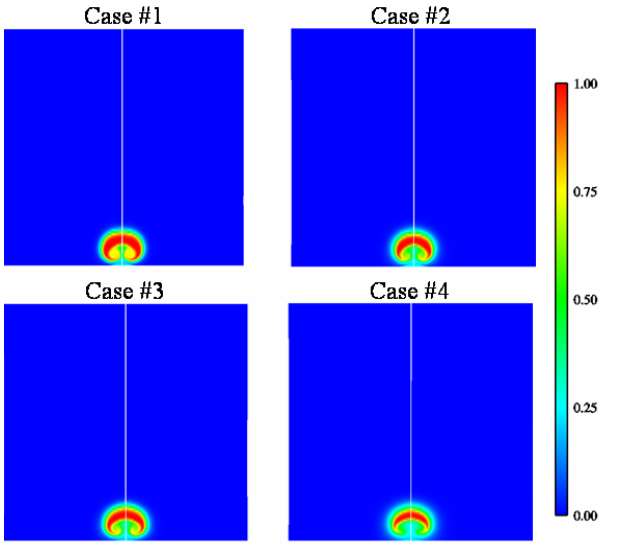

(c). Y_{H_2}

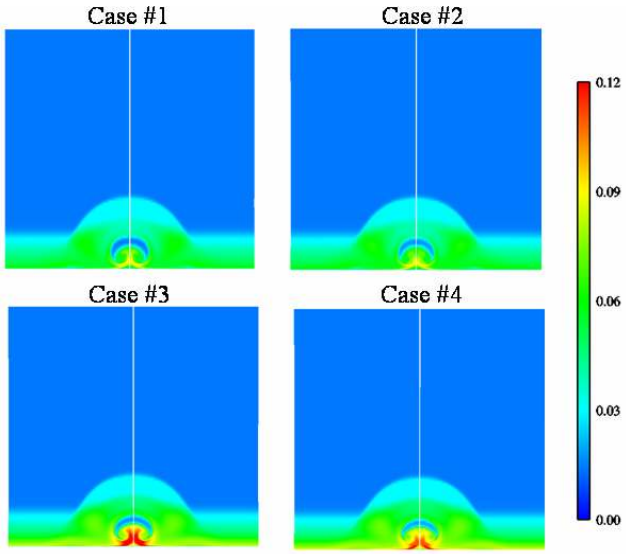

(d). $\sqrt{K}/u_\infty$

Figure 6. Contours at X=5 for the Constant Prandtl Number Simulations.

These figures all resemble the LES contours, but the turbulent kinetic energy levels for the cases with the compressibility correction off compare better to the LES calculation than the cases with the compressibility correction on. The contours of H_2 mass fraction, Y_{H2}, also show that the Case 4 closely matches the LES cutting plane contours. Comparing the temperature profiles for all the cases to the LES, it is seen that the LES has higher temperature values in the boundary layer and shock structure surrounding the jet. This was caused by the slightly different inflow profiles being used for the RANS and LES simulations. The RANS used the $1/7^{th}$ power law for velocity, and Crocco-Busemann for the temperature profile, while the LES used a recycling/rescaling technique.

B. Variable Prandtl / Schmidt Number Model

As described above, the variable Prandtl number model solves for the temperature variance and dissipation. The variable Schmidt number model additionally solves for the species variance and dissipation. From these two sets of quantities, the Prandtl and Schmidt numbers can be calculated. Figure 7 shows a comparison between the 2D simulation of this case by Brinkman [1] (transverse slot jet, rather than a discrete jet from a square duct) and the 3D simulation presented here for the normalized temperature fluctuation. For the 2D case, all the mixing occurs in the shear layer between the hot air stream and the cooler fuel, and in the separation zone that forms upstream of the jet. These areas show high values of the temperature fluctuation. Between the shear layer and the channel wall, there is no mechanism in the 2D flow to mix the fuel and air, so little to no temperature fluctuation is seen. The 3D simulation, taken down the centerline of the jet, shows the high values as the jet initially flows in the channel. The horseshoe vortex provides a mixing mechanism for the jet, which allows fluctuations across the fuel jet. Allowing for the differences in the 2D versus 3D nature of the flowfield, these simulations compare well to each other in the general structure of the temperature fluctuation field. However, the 3D has greatly enhanced turbulent kinetic energy due to the vortical mixing which alters all the fluctuation levels and flow structure.

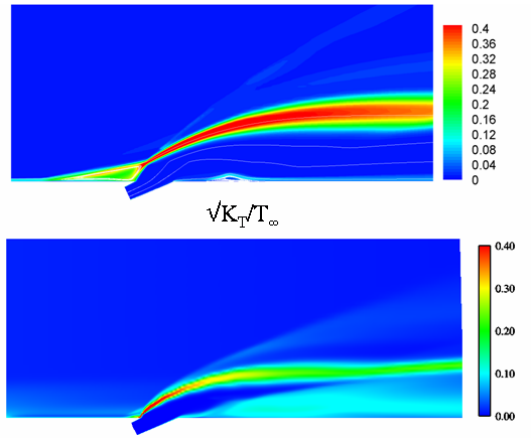

Figure 7. Temperature Fluctuation Comparison between 2D (top) and 3D (bottom) Models.

Table 4 lists the two Cases, 5 and 6, which were performed for this study. Both of these cases use the variable Prandtl and Schmidt number models, but Case 5 has the compressibility correction on and Case 6 does not. Figure 8 shows the oxygen entrainment for these cases, compared to the LES and to Case 1, which had compressibility, and a constant Lewis number of 1. The trend seen in the previous entrainment plot, that turning the compressibility correction off increases the mixing, is seen in this plot as well. The magnitude of the increase is not as great, and could be due to the coupling of the turbulence through the scalar variance equations.

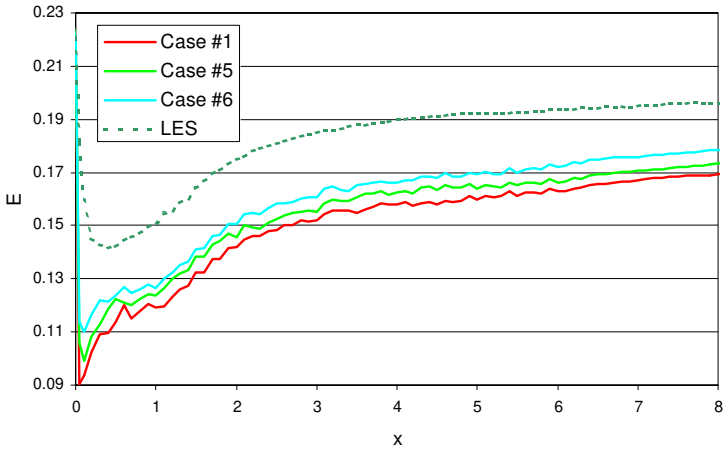

Figure 8. Entrainment for Variable Prandtl Number Model.

Figure 9 shows a comparison of the x = 5 cutting plane between the LES simulation and Case 6. Shown are the velocity and turbulent kinetic energy, temperature and temperature fluctuation, and fuel species and species fluctuation. Case 6 was chosen over Case 5 since it was shown in the previous section that the cases with the compressibility correction not active compare better in turbulent kinetic energy to the LES simulation. This can be seen when examining Figure 9a. Figure 9b shows the temperature and temperature fluctuation. Both of these quantities compare well to the LES simulation, with the LES simulation having slightly higher values for the fluctuation. The fuel species and fluctuation in Figure 9c also compare well in shape. The LES simulation has about double the value of the fluctuation compared to the RANS calculation. Since the Schmidt number is proportional to the square root of the reciprocal of the species fluctuation, the higher species fluctuation in the LES simulation would translate into a lower Schmidt number. The lower Schmidt number causes more species diffusion, which is represented in figure 9c by the less red area of the species mass fraction.

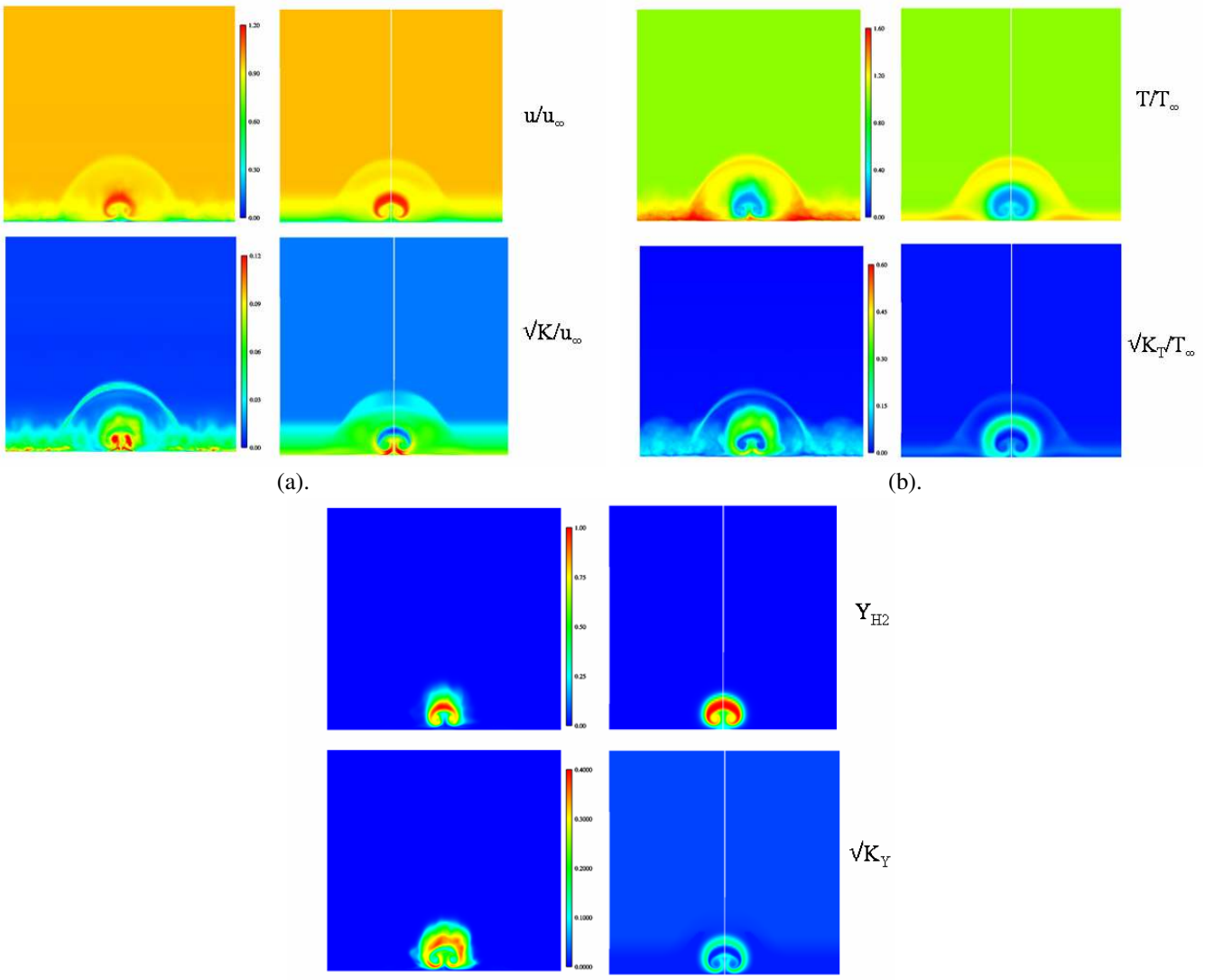

Figure 9. Comparison of the RANS Variable Prandtl / Schmidt Number Model to LES.

Figures 10 and 11 show the jet centerline view and x = 5 cutting plane view of the Prandtl, Schmidt, and Lewis numbers. The Prandtl number varies between 0.4 – 0.9 in the fuel jet region. The Schmidt number also varied in the jet region, with values ranging from 1.2 – 0.6. The lower values occurred in the top shear region of the jet, with higher values around the interior of the jet. The core region of the vortex had low values. The regions where the most mixing occurred had the lowest values, since this is where the species fluctuation would be greatest. The Lewis

number, which is Pr_t / Sc_t has values near 2 in the outer regions of the fuel jet close to the injection point, and these high values decrease as the jet propagates downstream. The interior of the jet has values that range from 0.5 to 1.0, with a large portion of the jet being in the 1.0 region.

These studies are preliminary. The scalar fluctuation model, calibrated by very basic unit problem data sets[1], is certainly operating in a qualitatively proper manner for a 3D fuel jet problem of this complexity. The LES calculation itself can be taken as "correct", but is still not entirely converged.

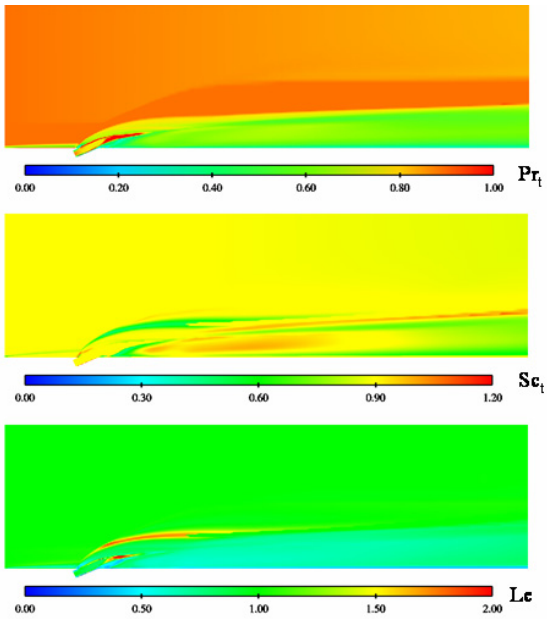

Figure 10. Variable Prandtl / Schmidt Number Model Centerline Profiles.

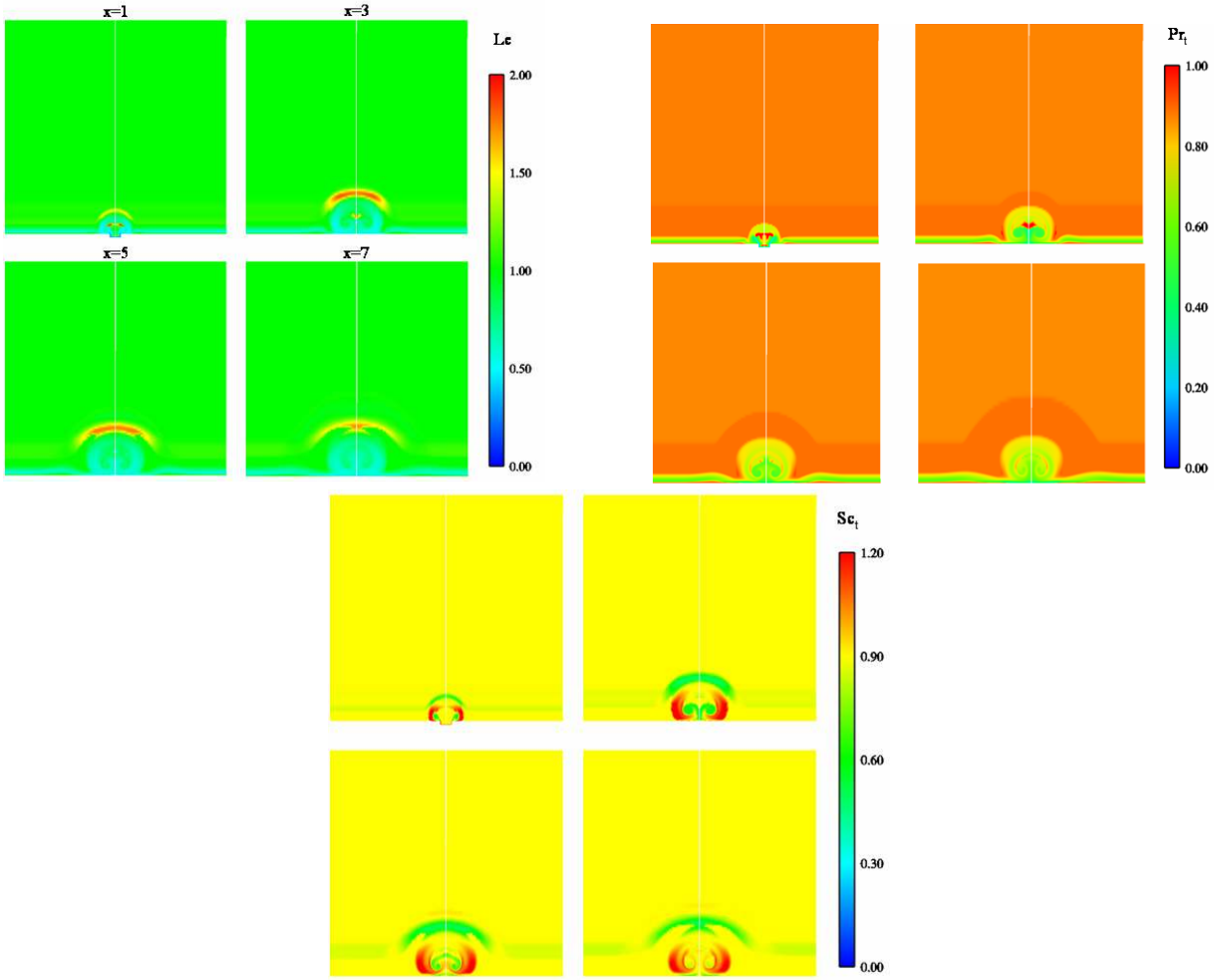

Figure 11. Variable Prandtl/Schmidt Number Model : Prandtl, Schmidt and Lewis Number Profiles.

V. RANS Simulations using CRUNCH CFD® Solver

The calculations performed in the above section were all done using a structured grid, RANS solver, CRAFT CFD®. In this section, results obtained using an unstructured solver CRUNCH CFD® will be exhibited. In many scramjet and fuel injector problems in general, the use of unstructured grids reduces the time and effort required to both grid certain geometries, and, more importantly, to obtain grid resolved solutions in a systematic and straightforward manner. For this problem, the use of a structured grid with one grid block required I-blanked regions. The same grid structure was used in the unstructured solver, but the I-blanked regions were not required, which reduced the grid size. The boundary layer inflow and jet inlet conditions between the two codes were nearly identical. Both codes had the Prandtl number constant at 0.9, a constant Lewis number at 1.0, and the compressibility correction activated. Figure 12 shows a comparison between the CRAFT CFD® and CRUNCH CFD® solvers. The vortex structure is slightly more bent about the centerline for the CRUNCH CFD® simulation, which can be seen in the velocity and species mass fraction contour plots. Overall, the two codes compared well to each other.

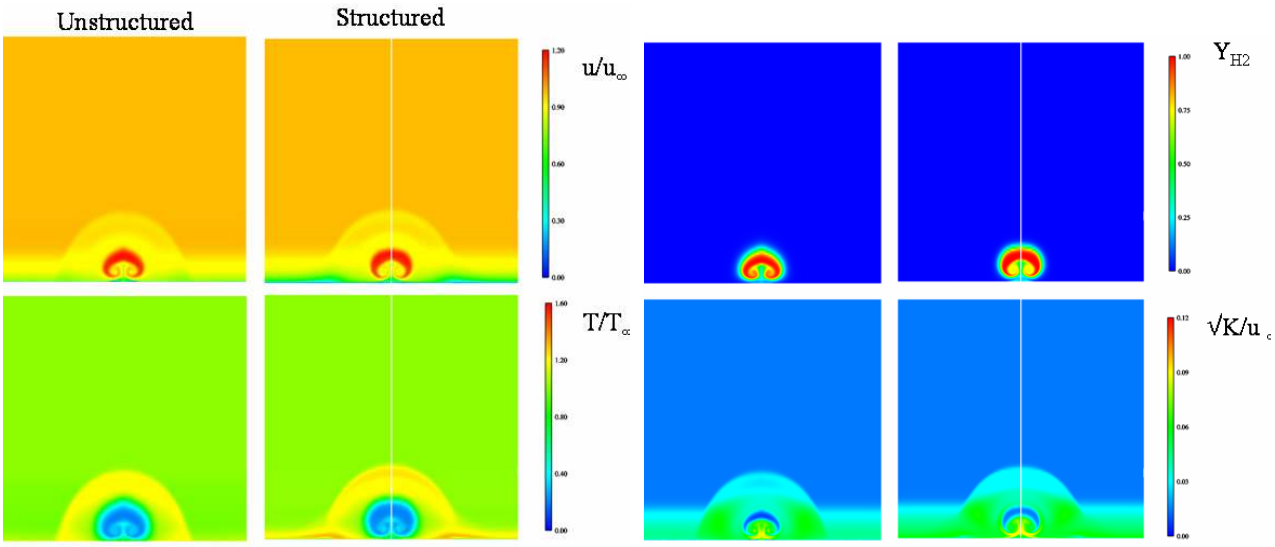

Figure 12. Comparison of the Unstructured (left) Solver to the Structured Solver (right) x = 5.0.

VI. Conclusions and Future Direction

In this study RANS simulations were performed and compared to an LES simulation on the same geometry. The LES simulation was computationally intensive and has progressed to a state where RMS mean flow quantities are converged but turbulent stresses and scalar variances are still somewhat noisy, but were yielding reasonable values. The first set of calculations performed examined the effects of varying the Lewis number while keeping the Prandtl number constant. These results showed that increasing the Lewis number resulted in greater mixing, but not to the levels of the LES simulation.

The next set of calculations performed examined the compressibility correction. It was determined that not having the correction active obtained results that were better than having the correction active. According to Spaid and Zukoski [15] for air injection into an air stream, the compressibility correction is required. A variation of this problem with Helium injection into an air stream [1] showed that the compressibility correction may not be adequate to capture the effects of the large air/Helium density gradient. One conclusion from this is that the compressibility correction may require a density modification to account for the interaction of different gases.

After these calculations were done, a new variable Prandtl and variable Schmidt number model, developed by was Brinkman [1] was used. This model showed that the Prandtl number varied from 0.4 to 0.9 in the jet region. The Schmidt number varied from 0.6 to 1.2, which created a Lewis number variation from 0.5 to 2.0 across the jet. The modeled temperature variance compared well in general shape and magnitude to the LES simulation. The species variance compared well in general shape, but had values that were about half those from the LES.

The final comparison was performed between the structured solver and unstructured solver on the same computational mesh. Both codes were run with the same Prandtl and Lewis numbers, but had slightly different

version of the compressibility correction. The comparison of mean flow quantities between the solvers is good. There is a slight difference in the shapes of the jets, with the unstructured solver having a more curved jet.

Acknowledgements

This work was supported by an Army program. Preparation of this paper has been accomplished with internal company funding. Thanks for the support from the NAVO HPC Center. I would like to thank fellow CRAFT Tech employees Jeremy Shipman and Greg Feldman who performed the unstructured computations. Thanks to Kathy Young for the preparation of this document. I also would like to thank Donald Kenzakowski, John Papp, and Ronald Ungewitter for the helpful discussions.

References

[1] Brinckman, K.W., Kenzakowski, D.C., and Dash, S.M., "Progress in Practical Scalar Fluctuation Modeling for High-Speed Aeropropulsive Flows," Paper No. AIAA-2005-0508, 43rd Aerospace Sciences Meeting and Exhibit, Reno, NV, Jan. 10-13, 2005.

[2] Kannepalli, C., Arunajatesan, S., and Dash, S.M., "RANS/LES Methodology For Supersonic Transverse Jet Interactions with Approach Flow," Paper No. AIAA-2002-1139, 40th AIAA Aerospace Sciences Meeting and Exhibit, Reno, NV, January 14-17, 2002.

[3] Ungewitter, R.J., Ott, J.D., Ahuja, V., and Dash, S.M., "CFD Capabilities for Hypersonic Scramjet Propulsive Flowpath Design," Paper No. AIAA-2004-4131, 40th AIAA/ASME/SAE/ASEE Joint Propulsion Conference and Exhibit, Fort Lauderdale, FL, July 11-14, 2004

[4] Sinha, N., Hosangadi, A. and Dash, S.M., "The CRAFT NS Code and Preliminary Applications to Steady/Unsteady Reacting, Multi-Phase Jet/Plume Flowfield Problems," 19th JANNAF Exhaust Plume Technology Meeting, CPIA Pub. 568, May 1991, pp. 203-226.

[5] White, F.M.., *"Viscous Fluid Flow,"* 2nd Edition, McGraw-Hill, Inc., New York, 1991.

[6] So, R. M. C., Zhang, H. S., and Speziale, C. G., "Near-Wall Modeling of the Dissipation Rate Equation", *AIAA Journal*, Vol. 29, No. 12, pp. 2069-2076, 1991.

[7] Sarkar, S., Dec. 1992, "The Pressure-Dilation Correlation in Compressible Flows", *Physics of Fluids, A*, Vol. 4 No. 12.

[8] Chidambaram N., Dash, S.M., and Kenzakowski, D.C., "Scalar Variance Transport in the Turbulence Modeling of Propulsive Jets," *Journal of Propulsion & Power*, Jan - Feb., 2001.

[9] Rai, M.M., and Moin, P.," Direct numerical simulation of transition and turbulence in spatially evolving boundary layer," *Journal of Computational Physics*, Vol. 109, pp.1 62-192, 1993.

[10] Rai, M.M., "Navier Stokes Simulations of Blade Vortex Interaction using High-Order Accurate Upwind Schemes, AIAA-87-0543, 1987.

[11] Smagorinsky, J., "General circulation experiments with the primitive equations, I, The Basic Experiment, *Monthly Weather Review,* 91,(3), pp.99-165, 1963.

[12] Menon, S., "Active Control of Combustion Instability in a Ramjet Using Large-Eddy Simulations," 29th AIAA Aerospace Sciences Meeting, Reno, NV, AIAA Paper 91-0411, 1991.

[13] Jameson, A., Schmidt, W., and Turkel, E., "Numerical Solutions of the Euler Equations by Finite Volume Methods Using Runge-Kutta Time-Stepping Schemes," AIAA 81-1259, June 1981.

[14] Baurle, R.A. and Eklund, D.R., "Analysis of Dual-Mode hydrocarbon Scramjet Operation at Mach 4-6.5, *J. of Propulsion and Power*, Vol. 18, No. 5, September-October, 2002.

[15] Spaid, F.W., and Zukoski, E.E., "A Study of the Interaction of Gaseous Jets from Transverse Slots with Supersonic External Flows," *AIAA Journal*, Vol. 6, No. 2, Feb 1968.